2-2016

MSH1 Is a Plant Organellar DNA Binding and Thylakoid Protein under Precise Spatial Regulation to Alter Development

Kamaldeep S. Virdi
University of Nebraska - Lincoln

Yashitola Wamboldt
University of Nebraska-Lincoln, ywamboldt2@unl.edu

Hardik Kundariya
University of Nebraska-Lincoln, kundariyahardik@unl.edu

John D. Laurie
University of Nebraska-Lincoln

Ido Keren
University of Nebraska-Lincoln

See next page for additional authors

Authors
Kamaldeep S. Virdi, Yashitola Wamboldt, Hardik Kundariya, John D. Laurie, Ido Keren, K.R. Sunil Kumar, Anna Block, Gilles J. Basset, Steve Luebker, Christian Elowsky, Philip M. Day, Johnna L. Roose, Terry M. Bricker, Thomas Elthon, and Sally A. Mackenzie

Molecular Plant
Research Article

CellPress
PARTNER JOURNAL

MSH1 Is a Plant Organellar DNA Binding and Thylakoid Protein under Precise Spatial Regulation to Alter Development

Kamaldeep S. Virdi[1,5], Yashitola Wamboldt[2,5], Hardik Kundariya[2], John D. Laurie[2], Ido Keren[2], K.R. Sunil Kumar[2], Anna Block[2], Gilles Basset[2], Steve Luebker[2], Christian Elowsky[3], Philip M. Day[2], Johnna L. Roose[4], Terry M. Bricker[4], Thomas Elthon[2] and Sally A. Mackenzie[2,*]

[1]School of Biological Sciences

[2]Department of Agronomy and Horticulture
University of Nebraska, Lincoln, NE 68588, USA

[3]Center for Biotechnology, University of Nebraska, Lincoln, NE 68588, USA

[4]Department of Biological Sciences, Louisiana State University, Baton Rouge, LA 70803, USA

[5]These authors contributed equally to this article.

***Correspondence: Sally A. Mackenzie (smackenzie2@unl.edu)**

http://dx.doi.org/10.1016/j.molp.2015.10.011

ABSTRACT

As metabolic centers, plant organelles participate in maintenance, defense, and signaling. MSH1 is a plant-specific protein involved in organellar genome stability in mitochondria and plastids. Plastid depletion of MSH1 causes heritable, non-genetic changes in development and DNA methylation. We investigated the *msh1* phenotype using hemi-complementation mutants and transgene-null segregants from RNAi suppression lines to sub-compartmentalize MSH1 effects. We show that MSH1 expression is spatially regulated, specifically localizing to plastids within the epidermis and vascular parenchyma. The protein binds DNA and localizes to plastid and mitochondrial nucleoids, but fractionation and protein–protein interactions data indicate that MSH1 also associates with the thylakoid membrane. Plastid MSH1 depletion results in variegation, abiotic stress tolerance, variable growth rate, and delayed maturity. Depletion from mitochondria results in 7%–10% of plants altered in leaf morphology, heat tolerance, and mitochondrial genome stability. MSH1 does not localize within the nucleus directly, but plastid depletion produces non-genetic changes in flowering time, maturation, and growth rate that are heritable independent of MSH1. MSH1 depletion alters non-photoactive redox behavior in plastids and a sub-set of mitochondrially altered lines. Ectopic expression produces deleterious effects, underlining its strict expression control. Unraveling the complexity of the MSH1 effect offers insight into triggers of plant-specific, transgenerational adaptation behaviors.

Key words: Thylakoid protein, Organellar DNA binding, MSH1, Epigenetic variation

Virdi K.S., Wamboldt Y., Kundariya H., Laurie J.D., Keren I., Kumar K.R.S., Block A., Basset G., Luebker S., Elowsky C., Day P.M., Roose J.L., Bricker T.M., Elthon T., and Mackenzie S.A. (2016). MSH1 Is a Plant Organellar DNA Binding and Thylakoid Protein under Precise Spatial Regulation to Alter Development. Mol. Plant. **9**, 245–260.

INTRODUCTION

Environmental stress elicits rapid and profound responses in plants designed for protection, avoidance, or progeny survival through changes in conditions. Many of the pathways that participate in these adaptive responses are influenced or controlled by epigenetic variations in the cell, involving small RNA, chromatin modification, and cytosine methylation changes (Eichten et al., 2014). Genes encoding DNA methylation machinery in plants are influenced in their expression by environmental cues (Boyko et al., 2010; Pecinka et al., 2010; Bilichak et al., 2012). Moreover, small RNAs can be transmitted systemically, permitting dissemination of these changes throughout the plant (Melnyk et al., 2011; Shivaprasad et al., 2012; Bond and

Published by the Molecular Plant Shanghai Editorial Office in association with Cell Press, an imprint of Elsevier Inc., on behalf of CSPB and IPPE, SIBS, CAS.

Baulcombe, 2014). Reprogramming of the methylome can produce changes that are transmitted through the gamete, perhaps a key capacity to predispose the next generation for enhanced stress response.

Many of the metabolic and developmental pathways that participate in plant adaptation intersect within the plastid (Rolland et al., 2012). This includes phytohormone and lipid metabolic processes, light- and daylength-responsive flower induction processes, plant biotic defense, and redox response. Likewise, heat tolerance (Kim et al., 2012), cytoplasmic male sterility (facultative gynodioesy; Hu et al., 2014), and oxidative stress response (Jacoby et al., 2012) are controlled by the mitochondrion. Because both epigenetic and organellar changes are often maternally transmitted, it is difficult to dissect their relative contributions to adaptive behaviors or to investigate their possible interrelationship. Yet there exists compelling evidence that organelles serve as key environmental sensors (Pfalz et al., 2012; Schwarzländer and Finkemeier, 2013), suggesting that they could participate directly in the signaling of programmed epigenetic responses.

MSH1 represents an unusual system that interlinks both organellar and heritable, non-genetic effects. The *MSH1* gene is unique to plants, encoding a protein that is dually targeted to both mitochondria and plastids (Abdelnoor et al., 2003; Xu et al., 2011). The MSH1 protein sequence is composed of at least six conserved domains, three presumably involved in DNA binding and regulation of recombination (Abdelnoor et al., 2006; Davila et al., 2011). Disruption or suppression of *MSH1* expression results in altered organellar genome stability (Davila et al., 2011; Xu et al., 2011), together with a process of developmental reprogramming that includes changes in numerous pathways affecting growth rate, flowering time, transition from juvenility, and abiotic stress responses (Xu et al., 2012).

Genome-wide methylome changes that characterize the *msh1* mutant are indicative of broader epigenetic effects (Virdi et al., 2015). While loss of MSH1 in the plant produces developmental reprogramming, reciprocal crossing of the reprogrammed plant to wild-type and selection of restored *MSH1/MSH1* genotype produces plant lineages with novel DNA methylome profiles and markedly enhanced and heritable growth vigor over wild-type (Virdi et al., 2015). Recent experiments demonstrate that these enhanced-growth effects are reproducibly transmitted through grafting (Virdi et al., 2015), implying that methylome reprogramming is mediated, at least in part, by small RNAs. These growth effects are recapitulated in other plant species by MSH1 RNAi suppression (Santamaria et al., 2014; Yang et al., 2015), reinforcing the argument that organellar and epigenetic effects of *MSH1* manipulation are conserved in plants.

Hemi-complementation experiments designed to effect mitochondrial versus plastid complementation of *MSH1* function in the mutant reveal distinct organellar contributions to the phenotype (Xu et al., 2012). Coupled with RNAi suppression experiments, the MSH1 effect can be dissected to its relative plastid, mitochondrial, and epigenetic contributions to developmental reprogramming. Here we describe the relationship of mitochondrial, plastid, and nuclear epigenetic changes following loss of *MSH1* expression. We show that MSH1 localizes to the nucleoid and thylakoid membrane of a specialized plastid type, appearing to associate with particular photosynthesis/stress-related components. *MSH1* perturbation or overexpression in the plastid produces redox changes in the plant that may be important in triggering the epigenetic response. MSH1 depletion in the mitochondrion leads to mitochondrial genome alteration and, at low frequency, combined heat tolerance, reduced seed germination, and altered leaf morphology. The epigenetic effects in *msh1* are separable from organellar effects, and integrate into the final *msh1* phenotype. Specialized localization and expression features of MSH1, coupled with mutation and gene-suppression behaviors, implicate MSH1 as a novel organellar component of environmental sensing and stress signal transmission in the plant.

RESULTS

MSH1-Associated Developmental Reprogramming Represents a Complex, Inter-organellar Integration Phenotype

We reported earlier (Xu et al., 2012) that hemi-complementation of plastid function in the *msh1* mutant (mitochondrial depletion of MSH1) produces normal-appearing plants showing little or no altered growth phenotype. In approximately 7%–10% of the plants, however, two unusual phenotypes occur. The first, termed ‘‘curly leaf,’’ is characterized by plants with downward curling of leaves showing a smooth surface, as shown in Figure 1A. Progeny of a curly leaf type display 100% penetrance of the phenotype in subsequent generations (Supplemental Tables 1 and 2).

The second phenotype is termed ‘‘wrinkled leaf,’’ and displays an unevenly ridged, bumpy leaf surface and dramatically altered leaf shape (Figure 1A). The wrinkled leaf phenotype ranges in intensity, with plants that display the most intense alterations producing few or no progeny. The phenotype is incompletely penetrant in subsequent generations (37.50%–89.47%), sometimes giving rise to curly leaf types as well (Supplemental Tables 1 and 2). In both curly and wrinkled leaf types, reciprocal crossing to wild-type demonstrates maternal transmission of the altered phenotypes (Supplemental Figure 1), and both show evidence of plastid-localized MSH1 (Figure 1B) and mitochondrial genome rearrangements (Figure 1C), confirming that the phenotypes arise as mitochondrial genetic effects. Both types also display evidence of enhanced heat tolerance (Figure 2A–2C), with reduced seed germination in the curly types (Figure 2D and 2E). Both curly and wrinkled leaf phenotypes are evident in the *msh1* mutant, and are not a consequence of the hemi-complementation process (Supplemental Figure 2).

Hemi-complementation of mitochondrial function in the *msh1* mutant (plastid depletion of MSH1) produces plants that are developmentally reprogrammed and display a range in intensity for leaf variegation, dwarfing, delay in juvenility–maturity transition (marked by rounded, juvenile leaf shape), and delay in flowering, similar to what was described in the earlier study of *msh1* (Supplemental Figure 3; Xu et al., 2012). This plastid-specific depletion of MSH1 also affects abiotic stress response, so that

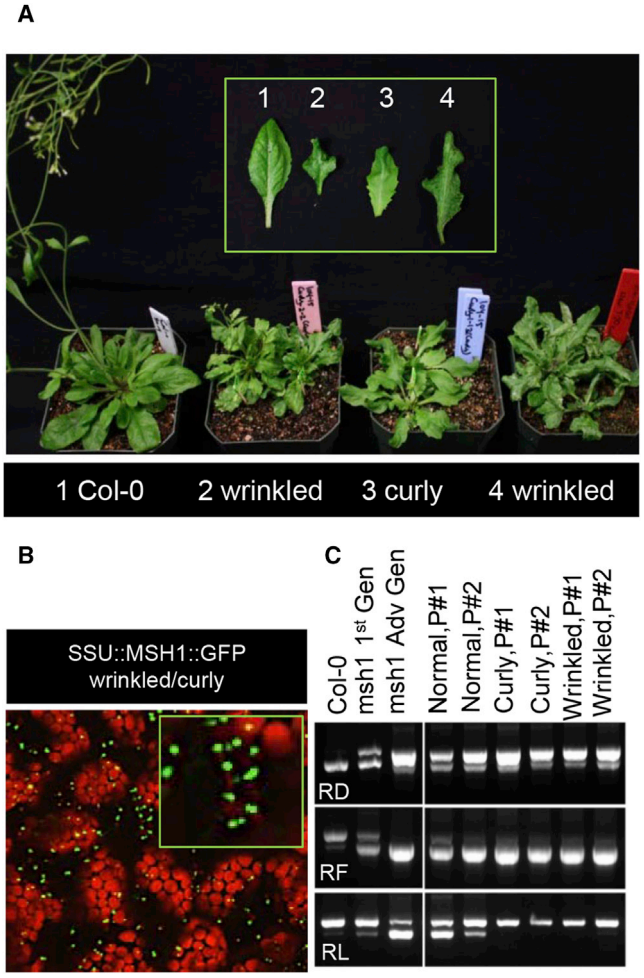

Figure 1. Characterization of SSU::MSH1 Wrinkled and Curly Leaf Plastid-Complemented Lines.

(A) Wrinkled and curly leaf phenotypes from SSU::MSH1::GFP hemi-complemented plants.

(B) Laser scanning confocal micrograph of wrinkled SSU::MSH1 hemi-complemented line expressing plastidial form of MSH1::GFP.

(C) PCR-based assay of mitochondrial DNA recombination in SSU::MSH1 normal, curly, and wrinkled lines. P# denotes plant number. Controls include the *msh1* mutant in first generation and advanced generation. Col-0, wild-type. RD, RF, and RL denote repeats D, F, and L as described in Arrieta-Montiel et al. (2009). Note differences in "normal" versus curly or wrinkled for Repeat L.

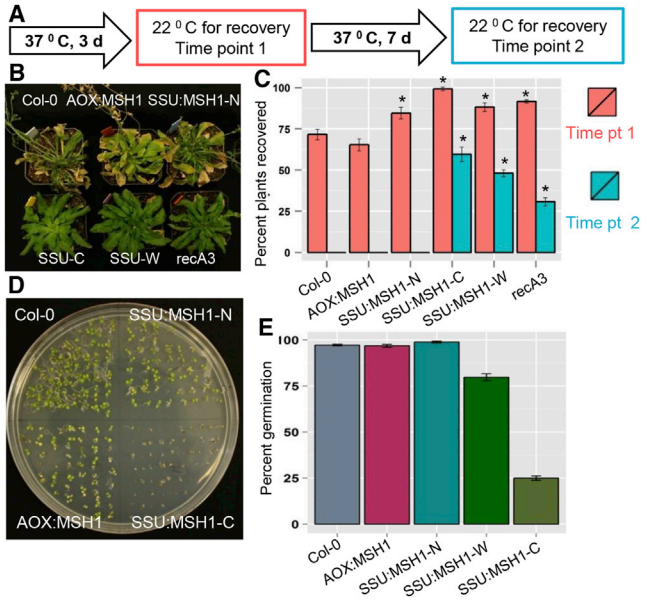

Figure 2. Heat Tolerance and Seed Germination Phenotypes in Altered Curly and Wrinkled Leaf Types.

(A–C) Mitochondrial hemi-complemented lines classified as curly or wrinkled were subjected to one of two heat treatments. Plant recovery at time point 1 is shown in **(B)**, with percentage of recovered individuals shown in **(C)**. AOX:MSH1 designates a mitochondria-complemented line, *recA3* is a mutant shown previously to display mitochondria-associated heat tolerance (Shedge et al., 2010), and SSU:MSH1 normal, curly (C), and wrinkled (W) are the three phenotypes emerging from plastid-targeted hemi-complementation. Data are presented from 15 plants each line. ANOVA and Tukey HSD (*$p < 0.001$ compared with Col-0) were performed on time point 1 and time point 2 separately. Error bars represent SD from three replications.

(D and E) Seed germination phenotype associated with the curly leaf types (SSU:MSH1-C), relative to wild-type (Col-0), the normal plastid hemi-complementation types (SSU:MSH1-N), and mitochondrial hemi-complementation line (AOX:MSH1). Seed germination data are shown in **(E)**. Error bars represent the SD of three replications.

hemi-complementation lines are, perhaps by their slower growth, more drought tolerant (Figure 3) and, by virtue of their variegation, more tolerant to high light stress (Xu et al., 2011). These observations are consistent with the *msh1* developmental reprogramming phenotype as an integration of both mitochondrial- and plastid-mediated behaviors.

Plastid and Low-Frequency Mitochondrial Disruption by MSH1 Depletion Alter Redox-Regulating Metabolite Physiology

While profound changes in plastid behavior were observed with depletion of MSH1, no significant differences between wild-type and the *msh1* mutant were apparent in amounts, oxidation rates, and reduction rates of the cytochrome *b6/f* complex or P700, and no major defects were observed in O-J-I-P fluorescence induction curves for assessing efficiency of photosystem II (PSII) closure (Methods as described by Roose et al., 2014). The *msh1* mutant produces a variegated phenotype. Dissected yellow sectors show increased levels of non-photoactive plastoquinone in reduced form (Xu et al., 2012), a feature that is generally characteristic of plants undergoing senescence (Besagni and Kessler, 2013). Furthermore, variegated tissues of the *msh1* mutant show an unusually high level of the demethylated precursor to phylloquinone (Xu et al., 2012), which distinguishes it from other variegation mutants in *Arabidopsis*. We therefore extended our analysis of physiological changes in *msh1* and hemi-complementation lines.

In green tissues, *msh1* mutants displayed elevated, more highly reduced plastoquinone levels than in wild-type (Figure 4A), with the effect more pronounced in the stem than the leaf (Figure 4D). Similarly, plastochromanol-8 and α-tocopherol levels were higher in the stem of *msh1* plants relative to

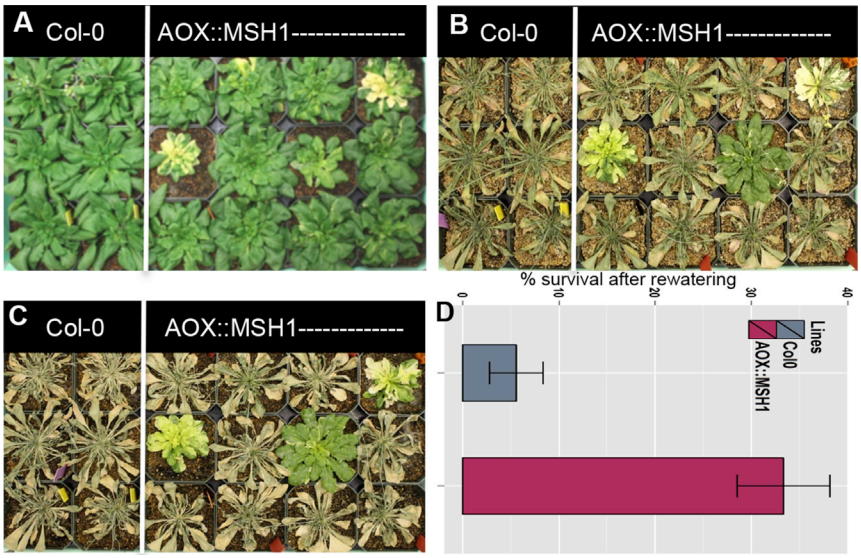

Figure 3. Response of Plastid-Perturbed Plants to Moisture Depletion.
(A) Hemi-complementation line containing a mitochondrially targeted form of *MSH1* grown 28 days at 12-h photoperiod and 22°C in controlled growth room.
(B) Plants subjected to 14 days without watering in the same growth room.
(C) Recovery following watering.
(D) Percent survival following watering. Data from three replications, 12 plants each.

wild-type (Figure 4E and 4F). The *msh1* mutant showed enhanced non-photochemical quenching rates in the light, followed by slower decay rates in the dark (Supplemental Figure 4).

An *MSH1* overexpression line was developed by stable transformation of Col-0 wild-type plants with an *MSH1* native promoter::*MSH1* full-length gene::GFP (green fluorescent protein) construction. Overexpression of *MSH1* results in an unusual leaf-yellowing phenotype, delayed flowering, MSH1 accumulation in mesophyll plastids, and altered plastid morphologies including enhanced plastoglobule accumulation and size as a likely sign of plastid stress (Figure 4G–4J). Overexpression of MSH1 results in physiological effects strikingly similar to those of the *msh1* mutant for plastoquinone, plastochromanol-8, and α-tocopherol levels in the stem, together with exaggerated levels of these metabolites in the leaf (Figure 4A–4F). Overexpression studies with CaMV35S::MSH1::GFP introduced to Col-0 wild-type plants produced high-frequency gene co-suppression and the *msh1* mutant phenotype (Supplemental Figure 5). Thus we conclude that high-level, ectopic *MSH1* expression is not tolerated by the system, and even mild overexpression under native promoter produces deleterious growth effects. The observation of *MSH1* co-suppression may also be indication of endogenous epigenetic regulation of *MSH1*.

Hemi-complementation tests showed that the altered redox behavior in *msh1* was conditioned by plastid perturbation (Supplemental Figure 6A). Plastid-complemented *msh1* mutants showed no alteration in redox-associated metabolite behavior, while mitochondrially targeted MSH1 (plastid depletion) showed effects similar to those described for the *msh1* mutant. However, assays of the low-frequency curly and wrinkled leaf hemi-complementation lines, depleted in mitochondrial MSH1, produced plastid metabolite changes similar to those in *msh1*, indicating that mitochondrial dysfunction can also lead to plastid redox stress response (Supplemental Figure 6A). These results show that *msh1* organellar perturbation in either plastid (high frequency) or mitochondrion (at lower frequency) creates a similar stress state that we suspect to be relevant to epigenetic reprogramming.

MSH1 Expression Is Spatially Regulated

The more pronounced redox metabolite modulation in the stem than leaves of *msh1* suggests that *MSH1* is spatially regulated in its expression. To examine expression timing, the *MSH1* promoter was fused to β-glucuronidase (*uidA*) and stably transformed to *Arabidopsis* ecotype Col-0. While signal was detected in nearly all plant tissues throughout development, the spatial pattern of expression was restricted to epidermal cells, vascular parenchyma, meristems, and reproductive tissues (Figure 5). This expression pattern was confirmed with gene constructions that included the *MSH1* promoter and full-length gene fused to GFP (Figure 6). Homozygous *msh1*-complemented lines (Xu et al., 2011) were used for this study to ensure proper functional localization. These experiments show that the unusual spatial pattern of MSH1 accumulation is promoter driven.

Analysis by laser scanning confocal microscopy in the leaf lamina region showed GFP signal positioned on the upper layer of cells. However, near the midrib, the signal was detected in nearly all cell layers (Figure 6A–6D). At higher magnification, one is able to observe GFP as punctate signals within plastid structures visibly smaller than mesophyll chloroplasts (Figure 6A and 6C). These plastid structures showed only muted autofluorescence relative to mesophyll chloroplasts, implying lower chlorophyll levels. To unambiguously distinguish the small plastids from mitochondria, we confirmed that a plastid hemi-complemented line, in which native promoter-driven MSH1 targets only to plastids, produced the same expression pattern.

MSH1 Is Localized to a Special Plastid Type

The size of MSH1-containing plastids is more readily estimated by electron microscopy, whereby the smaller plastids are approximately 30% the size of mesophyll chloroplasts in neighboring cells (Figure 7). The smaller, MSH1-associated plastids display less extensive thylakoid membrane and granal stacking, and contain fewer visible plastoglobules than do mesophyll chloroplasts (Figure 7A–7D). While their autofluorescence signal is lower than that of mesophyll chloroplasts, they contain visible starch. Epidermal plastids have the capacity to synthesize starch from imported carbohydrates rather than by their own photosynthetic activity (Tsai et al., 2009).

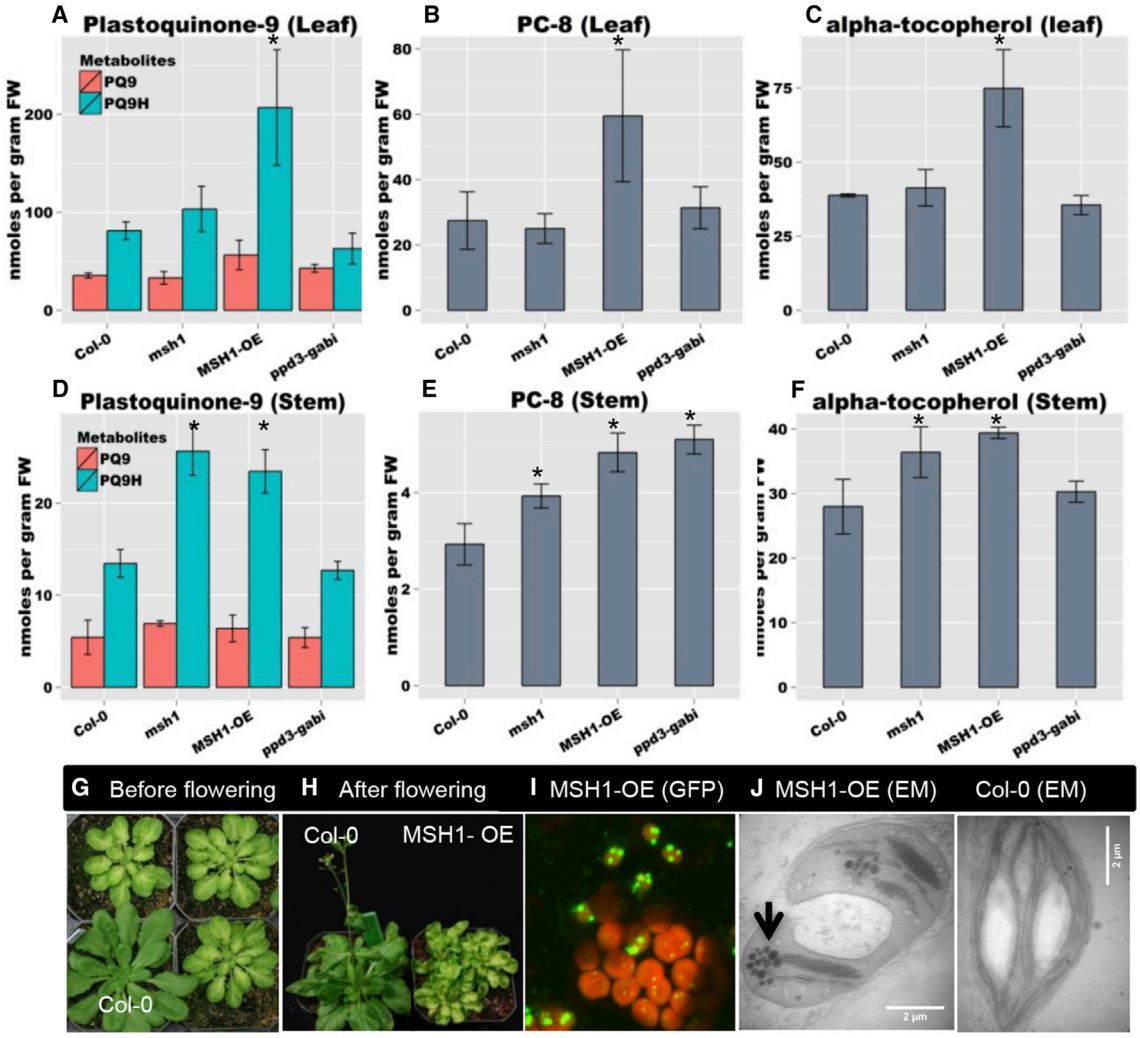

Figure 4. Physiological Changes Associated with MSH1 Disruption.

Level of total plastoquinone-9 **(A and D)**, plastochromanol-8 **(B and E)**, and α-tocopherol **(C and F)** from leaf and stem of Col-0, *msh1, ppd3*, and MSH1 overexpression (OE) lines. Test of significance was done by ANOVA and Tukey HSD. Error bars represent SD from four replications. * $P \leq 0.05$; ** $P \leq 0.01$.

(G) Comparison of growth phenotype in Col-0 and MSH1-OE lines derived by introducing the native promoter:MSH1:GFP construction to a wild-type Col-0 line.

(H) The MSH1-OE lines display evidence of slower growth rate and delayed flowering.

(I) Laser confocal micrograph shows ectopic MSH1 accumulation in both epidermal and mesophyll plastids in the MSH1-OE line.

(J) Transmission electron micrograph of an aberrant plastid in the MSH1-OE line and Col-0. Note the increase in number and size of plastoglobules in MSH1-OE (arrow) compared with Col-0. Scale bar, 2 µm.

To learn whether these organelles, and their unusual association with MSH1, can be generalized to other plant species, we stably transformed the *Arabidopsis* MSH1::GFP gene construct into tobacco (*Nicotiana tabacum* L). Confocal microscopy in tobacco revealed a similar pattern of smaller organelles in epidermal and vascular parenchyma cells, as well as association of MSH1 to these organelles in punctate patterns (Figure 7E and 7F). In both *Arabidopsis* and tobacco, crude plastid preparations were analyzed by fluorescence-activated cell sorting (FACS) to estimate the fraction of plastids that contain the protein. Results from these experiments indicate that MSH1-expressing plastids comprise approximately 2%–3% of total intact plastids isolated from leaves, and 12%–14% in stems (Supplemental Figure 7). These observations would account for the predominance of redox-associated effects detected in the *msh1* stem.

MSH1 Appears to Be a DNA Binding Protein

The punctate GFP signal observed within the MSH1-associated plastids indicates that at least some portion of MSH1 is sub-compartmentalized within these organelles. GFP-punctate structures within the plastids may be nucleoids (Terasawa and Sato, 2005) or plastoglobules (Vidi et al., 2006). We previously showed that punctate MSH1::GFP signals in plastids co-localized with DAPI staining in a few cells (Xu et al., 2011). DNA binding feature predictions within the protein sequence and *MSH1* association with mitochondrial DNA recombination activity (Davila et al.,

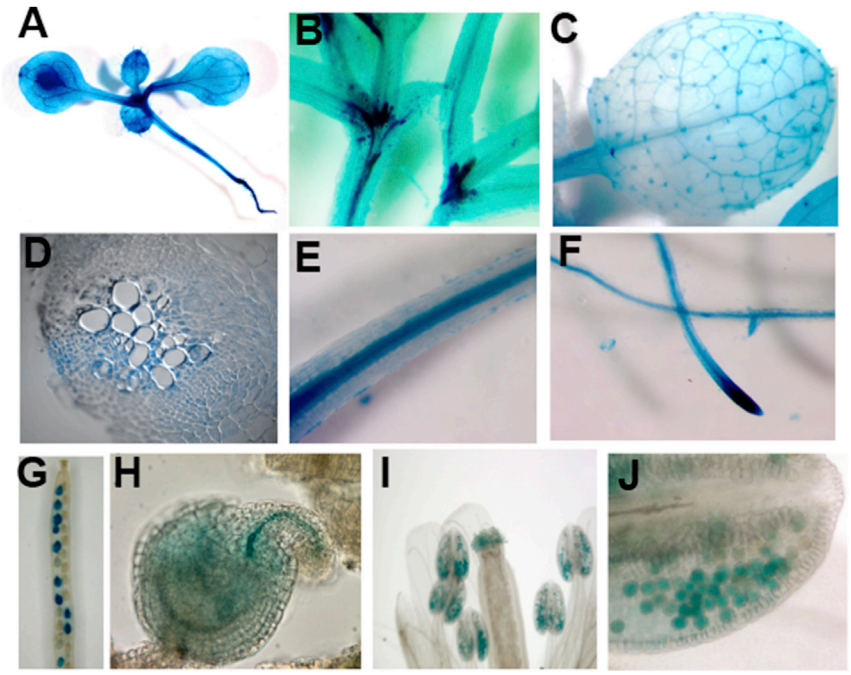

Figure 5. *MSH1* Expression with GUS Reporter.
(A) Seedling of stable Col-0 transformant containing a gene construction comprising *MSH1* native promoter fused to β-glucuronidase.
(B) Seedling sectioned to expose meristem.
(C) Expression in veins and trichomes of young rosette leaf.
(D) Leaf midrib cross section showing *MSH1* expression in the vascular parenchyma.
(E and F) Expression in vascular bundle of root **(E)** and root tip **(F)**.
(G–J) Ovules within silique **(G)**, ovule **(H)**, pollen within anthers **(I)**, and pollen **(J)**.

2011) imply nucleoid association. We therefore conducted transient co-infiltration and genetic complementation experiments. Co-infiltration and laser scanning confocal microscopy showed co-localization of MSH1::RFP (red fluorescent protein) with three confirmed nucleoid proteins, pTAC2, PEND and MFP1, each carboxy-tagged with GFP and displaying very similar punctate localization patterns (Figure 8A).

Locating to the nucleoid implies MSH1 association with the plastid genome, which was supported both by site-directed mutagenesis and chromatin immunoprecipitation (ChIP). The ChIP assay showed that selective pull-down of MSH1-GFP with anti-GFP antibodies was followed by successful amplification of three plastid genome encoded genes, consistent with MSH1 binding to plastid DNA (Figure 8E). Site-directed mutations were introduced to a putative FYE DNA binding motif present within *MSH1* domain I for functional assay by genetic complementation (Figure 8B; Supplemental Table 3).

Substitution of the highly conserved phenylalanine alone (FYE/LYE) produced a protein unable to complement the plastid-associated variegation phenotype as well as mitochondrial DNA recombination, reinforcing the model of MSH1 function within the nucleoid and in DNA binding in both organelles (Figure 8C, 8D, and 8F). The phenylalanine substitution in MSH1 still produced punctate signals within the sensory plastid (Figure 8G), suggesting that DNA binding is not required for nucleoid localization. Also, the phenylalanine substitution appeared to be sufficient to condition the full complexity of *msh1* phenotype, implying that DNA binding, or the protein conformation stemming from this binding, is essential to the protein's function.

Substitution of the less-conserved tyrosine (FYE/FCE) had no obvious effect on mitochondrial and plastid functions, and the mutation permitted complementation of *msh1* phenotypes (Figure 8C, 8D, and 8F). Substitution of the highly conserved glutamate (FYE/FYA) led to unexpected results. The mutant protein produced no detectable signal in plastids (Supplemental Figure 8), and negative complementation results. The mutation did not affect mitochondrial DNA stability, indicating that DNA binding and mitochondrial-targeting features of the protein remained intact. Thus, mutation of the glutamate does not appear to affect DNA binding, but is apparently essential for either targeting or protein stability within the plastid (Supplemental Figure 8). As further confirmation, the triple mutant FYE/LCA showed loss of MSH1 plastid localization, non-complementation of *msh1* phenotype, and increased mitochondrial DNA recombination (Supplemental Figure 8).

Mutant phenotypes produced by substitution of phenylalanine, which affects DNA binding but allows nucleoid localization of the protein, and glutamate, which prevents targeting or protein stability in the plastid altogether, were indistinguishable. This result argues for the essential nature of DNA binding not only in genome stability but also in developmental, stress, and epigenetic features of the MSH1 effect.

A series of *MSH1* nested deletions was developed to delimit, beyond domain I, the protein interval necessary for nucleoid targeting and protein function. These experiments, summarized in Supplemental Figure 9, showed that in addition to domain I, domain II and the hydrophobic interval of domain III appear to be essential for protein localization to the nucleoid. Likewise, deletion analysis showed that domains I–V and domains II–VI are not sufficient for partial protein function; the full-length protein is required.

MSH1 Also Associates with the Thylakoid Membrane

Because MSH1 is in low abundance, we carried out cell fractionation experiments in an *Arabidopsis* stable MSH1-GFP transformant under control of its native promoter. *In silico* analysis of the MSH1 protein predicted three hydrophobic intervals (Supplemental Table 4), and plastid fractionations showed MSH1 co-purifying with the thylakoid membrane (Figure 9A). This association persisted with mild detergent, salt washes, or DNase treatments, implying that the protein is membrane-attached and

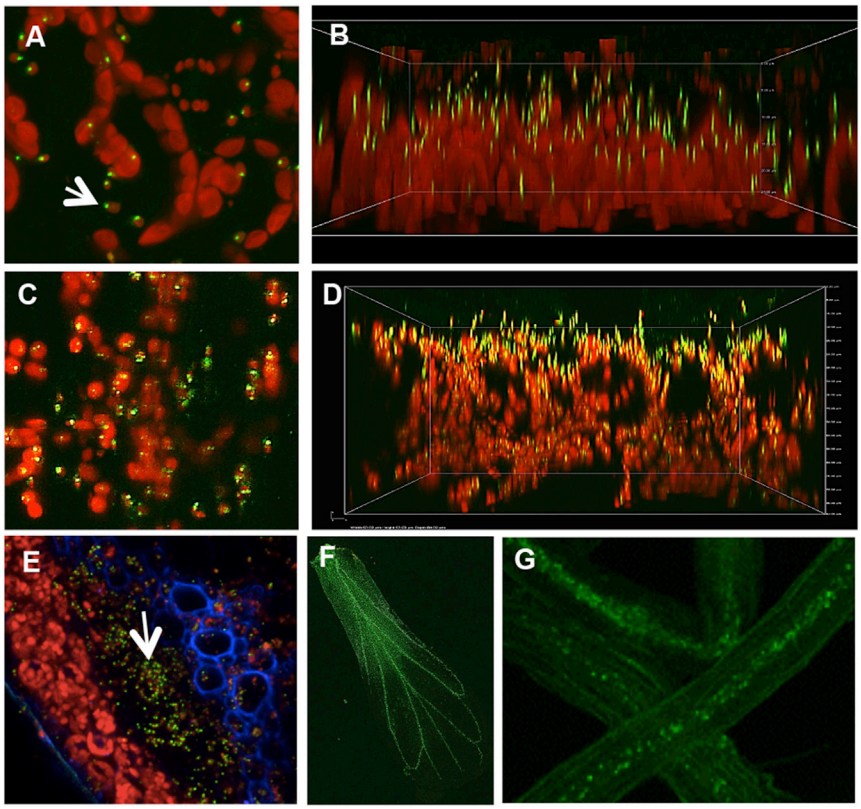

Figure 6. Spatial Localization of MSH1 within Plastids in *Arabidopsis*.
(A) GFP signal in small epidermal plastids. *Arabidopsis* genetic complementation with the MSH1:GFP transgene under control of the *MSH1* native promoter allows detection of *MSH1* expression by laser scanning confocal microscopy. Epidermal plastids (arrow) are smaller, oblong in shape, and lower in autofluorescence than the mesophyll chloroplasts seen as large, red organelles.
(B) Orthogonal view showing that MSH1 signals reside in surface epidermal plastids.
(C) MSH1 signal in both epidermal and vascular parenchyma plastids near leaf midvein.
(D) Orthogonal view near vein, with signal visible in upper and lower cells of the leaf.
(E) Cross section of inflorescence stem showing GFP signal (arrow) within vascular parenchyma cells of phloem (xylem in blue).
(F and G) flower petal **(F)** and roots **(G)** showing localization of MSH::GFP signal predominantly within vascular tissues.

not simply a component of the nucleoid (Figure 9B, 9C, and 9F). Although protein topology has not yet been fully elucidated, MSH1 co-fractionated with a high molecular weight complex (Figure 9D) believed to comprise the PSII–light-harvesting complex II supercomplex under protein non-denaturing conditions (Fristedt et al., 2015).

Yeast two-hybrid and co-immunoprecipitation (coIP) experiments identified putative MSH1 protein partners within the plastid. Initial yeast two-hybrid assays, with full-length *MSH1* as bait and a cDNA library prepared from whole above-ground plant tissue at flowering, identified at least 12 gene products as putative interaction partners (see Supplemental Table 5 for partial listing). We have focused on one of these, PPD3, for the present study. PPD3 is a 27.5-kDa PsbP domain-containing protein thought to reside in the thylakoid membrane and/or lumen (Friso et al., 2004; Bricker et al., 2013; Ifuku, 2014). CoIP experiments with MSH1 also produced PPD3 as a putative interaction partner (Figure 10).

MSH1 sub-divides into six conserved intervals based on cross-species protein alignments (Abdelnoor et al., 2006), with domain 1 containing the DNA binding/mismatch recognition domain, domain 5 an ATPase domain, and domain 6 a GIY-YIG endonuclease domain. Sub-cloning MSH1 in accordance with these intervals, we conducted yeast two-hybrid matings with each MSH1 domain as bait. From these experiments, positive interaction occurred with PPD3 at domains 2, 3, and 6. The nature of MSH1 association with the thylakoid membrane is not yet defined, although domain 3–4 is bordered on both sides by short hydrophobic intervals (Supplemental Table 4).

MSH1 and PPD3 Are Co-expressed and Appear to Be Functional Interaction Partners

Native promoter::PPD3::GFP fusion constructs were developed to test PPD3 expression and localization behavior. PPD3 produced punctate signals within small sized plastids in the epidermal layer and the vascular parenchyma similarly to MSH1, with no detected signal in mesophyll chloroplasts (Figure 10E and 10F). This was in contrast to PsbO1 and PsbO2, two control proteins that also reside within the PSII oxygen-evolving complex and produced signal in all plastids including mesophyll.

Experiments by others have suggested that some PSBO1 protein may reside within the plastoglobule (Vidi et al., 2006; Ytterberg et al., 2006), and this could perhaps be the case, though unconfirmed, for PPD3. The observed spatial expression pattern of *PPD3* would preclude its detection in plastoglobule preparations from whole leaf tissues. PPD3 expression appears to be suppressed by redox signals (Fey et al., 2005), similarly to MSH1, and there is some indication that PPD3 may be part of a stress response in the plant (Ifuku, 2014). Confocal microscopy of contrasting fluor-tagged MSH1 and PPD3 show overlap in their diffuse (membrane) signal, but not their punctate signal patterns (Figure 10H). We interpret this result to reflect the localization of MSH1, but not PPD3, within the nucleoid, and PPD3 and MSH1 interaction on or within the thylakoid membrane.

TDNA insertion mutants were obtained for PPD3 in *Arabidopsis*. The insertions were located at two sites in the gene, one in the promoter (*ppd3*-sail) and one in an exon (*ppd3*-gabi) (Supplemental Figure 10). TDNA insertion mutants produced no readily detectable changes in growth behavior of the plants grown under normal conditions. A small proportion (~10%) of *ppd3*-gabi plants, and their progeny, displayed a perennial-like growth behavior with aerial rosettes, similar to what is observed

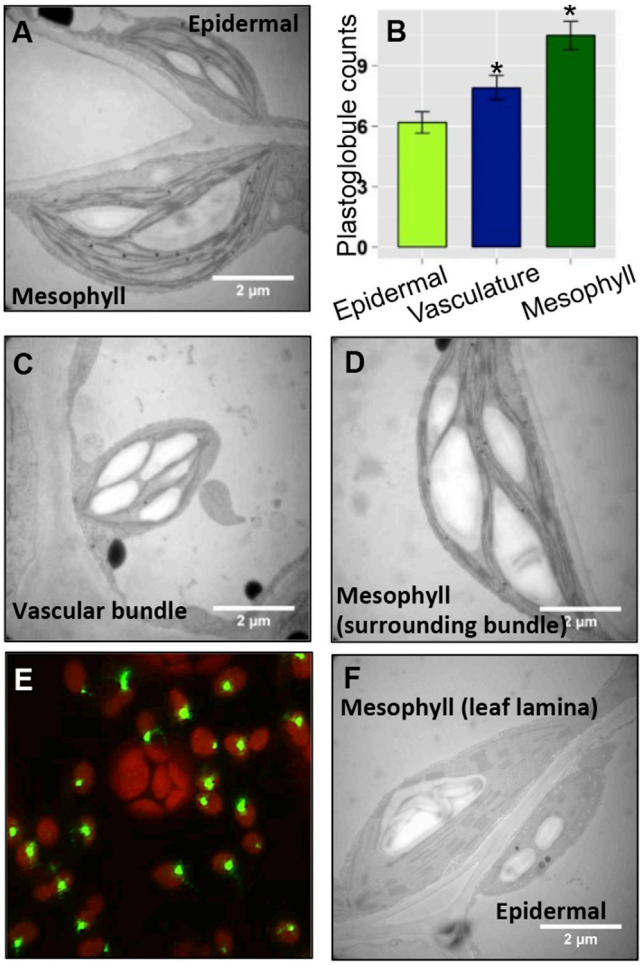

Figure 7. Morphology of the MSH1-Containing Plastid.

(A) Electron microscopy of leaf epidermal and mesophyll plastids from *Arabidopsis* wild-type Col-0. Epidermal plastids measure approximately 30% the size of mesophyll chloroplasts.

(B) Number of plastoglobules per electron microscopy section from 20–25 different fields of two independent samples. $P \leq 0.05$.

(C and D) Vascular bundle **(C)** and mesophyll surrounding bundle **(D)** from Col-0.

(E and F) Plastids from tobacco wild-type expressing MSH1::GFP under the *MSH1* native promoter **(E)**, with localization to epidermal plastids. Electron microscopy section from wild-type tobacco **(F)** displaying a similar size disparity between epidermal and mesophyll plastids.

Scale bars, 2 μm.

in the *msh1* mutant (Supplemental Figure 10D). Non-photochemical quenching level and redox status were also altered in *ppd3*-gabi lines similarly to *msh1* (Figure 4; Supplemental Figure 4). However, no mutant lines displayed a full *msh1*-like phenotype.

MSH1 Does Not Appear to Be a Nuclear Protein but Effects a Heritable, Epigenetic Phenotype

Earlier studies showed that MSH1 disruption or suppression is accompanied by heritable changes in nuclear cytosine methylation patterns (Virdi et al., 2015). These observations raise the possibility that MSH1 might also function within the nucleus of the cell. MSH1 hemi-complementation experiments that target the protein to the plastid and appear to fully complement *msh1* (Xu et al., 2012) show no evidence of MSH1 nuclear localization by confocal microscopy. An MSH1::GFP construction, encoding native promoter and substituting an ATG start codon in place of the MSH1 targeting presequence (Supplemental Figure 11A), produced a cytosolic protein (Supplemental Figure 11E). These experiments revealed no evidence of functional complementation for the *msh1* phenotype (Supplemental Figure 11B–11D). This was also the case when the CaMV 35S promoter was substituted for native promoter in a similar experiment.

Introduction of a nuclear localization signal (NLS) to the *MSH1* gene construction in place of the presequence produced nuclear-targeting MSH1 (Supplemental Figure 11F). However, this construction also produced no functional complementation (Supplemental Figure 11G). These results do not definitively rule out MSH1 function in the nucleus but, together with hemi-complementation data (Xu et al., 2011), suggest that any MSH1 nuclear association would likely occur via the plastid.

To dissect the epigenetic component of the *msh1* phenotype, we developed MSH1 RNAi suppression lines in *Arabidopsis* and, following the T1 generation, derived RNAi transgene-plus and -minus lines for further analysis. Lines containing the RNAi transgene displayed 50%–80% suppression of *MSH1* transcripts and the full *msh1* phenotype, including variegation and mitochondrial DNA recombination (Figure 11). Transgene-null lines displayed normal levels of *MSH1* transcript, and no longer displayed leaf variegation, a plastid genetic phenotype, or the curly leaf/wrinkled leaf phenotypes or mitochondrial DNA rearrangements diagnostic of mitochondrial genetic changes. In addition, transgene-null lines no longer displayed the altered redox metabolite changes characteristic of *msh1* (Supplemental Figure 6B). Instead, three out of seven transgene-null lines displayed heritable and uniform changes in delayed flowering, delayed juvenility transition, dwarfing, reduced leaf number, and lighter green leaf color (Figure 11A). These traits appear to constitute the epigenetic component of the *msh1* phenotype.

The *msh1* mutant is altered not only in phenotype but in crossing behavior. Crossing *msh1* reciprocally to wild-type Col-0 produces enhanced vigor phenotypes in a proportion of the *MSH1/MSH1* progeny, an effect that is particularly pronounced by the F3 and F4 generations (Virdi et al., 2015). Genome-wide cytosine methylation analysis of F3 enhanced-growth selections, termed epiF3, shows non-random changes in methylation pattern that are distinctive (Virdi et al., 2015).

The enhanced-growth effects from crossing an *msh1* mutant with wild-type are observed in reciprocal crosses, and so are non-organellar (Virdi et al., 2015). Earlier studies showed these growth effects to emanate from crossing plastid-perturbed lines (Virdi et al., 2015). However, similar growth effects may arise from crossing the curly/wrinkled leaf types that derive at low frequency from mitochondrially perturbed lines (Supplemental Figure 6C), implying that the redox metabolite changes may serve as a predictor of this enhanced-growth phenomenon. To further investigate the possibility of cytoplasmic influence on this MSH1 effect, we carried out two independent experiments. The first involved reciprocal crosses between first- and second-generation *msh1* mutants with the

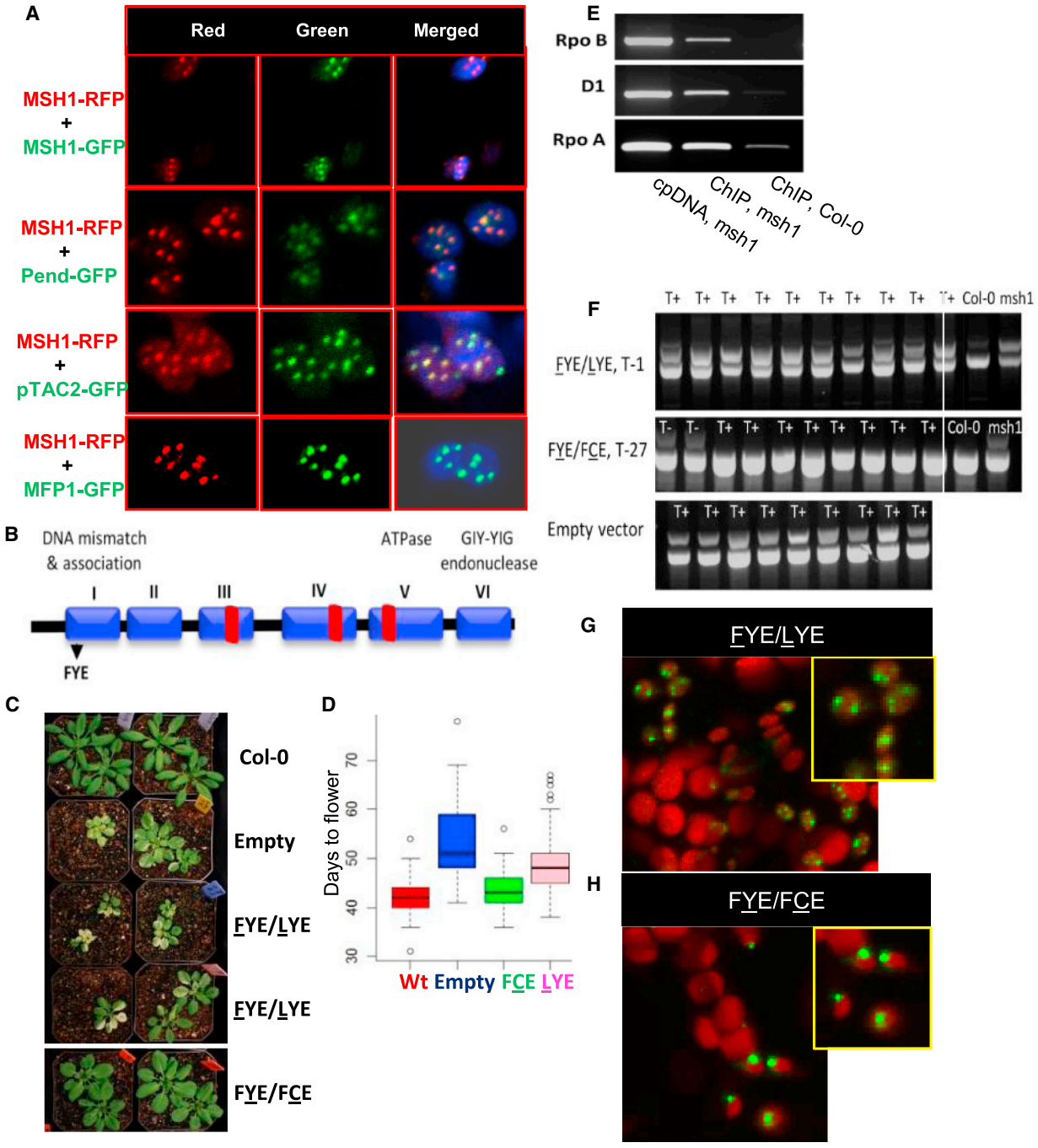

Figure 8. MSH1 Appears to Be a Plastid DNA Binding Protein and Phenylalanine is Essential for Its Function.

(A) Co-localization of MSH1 with nucleoid proteins by laser scanning confocal microscopy. Fluor-tagged gene constructs are indicated to the left of each panel at distinct wavelengths to allow resolution of RFP (red), GFP (green), and merged images. This experiment tests for co-localization of MSH1 and three known nucleoid proteins.

(B) Diagram of MSH1 protein consisting of six domains, three hydrophobic/transmembrane stretches (red bars), and FYE motif within DNA binding domain.

(C and D) Genetic complementation assay with FYE/LYE and FYE/FCE point mutations within MSH1 DNA binding domain, early stage **(C)** and days to flowering **(D)**. The complementation assay involves introduction of the test *MSH1* transgene construction to an *MSH1/msh1* heterozygote, followed by selection of the *msh1/msh1* progeny segregant containing the transgene.

(E) Plastid ChIP assay. DNA immunoprecipitation was carried out with anti-GFP beads, and PCR was run with primers specific for three plastid genome-specific genes. msh1 indicates that a MSH1::GFP complemented line was used.

(F) PCR-based mitochondrial DNA recombination assay results for the two DNA binding domain mutants. The double band pattern indicates that illegitimate recombination is occurring, an indication that the transgene does not complement the *msh1* phenotype.

(G and H) Confocal microscopy of stable transgenic lines containing FYE/LYE **(G)** or FYE/FCE **(H)** transgene to confirm that the altered MSH1::GFP constructs are targeted to the epidermal plastids.

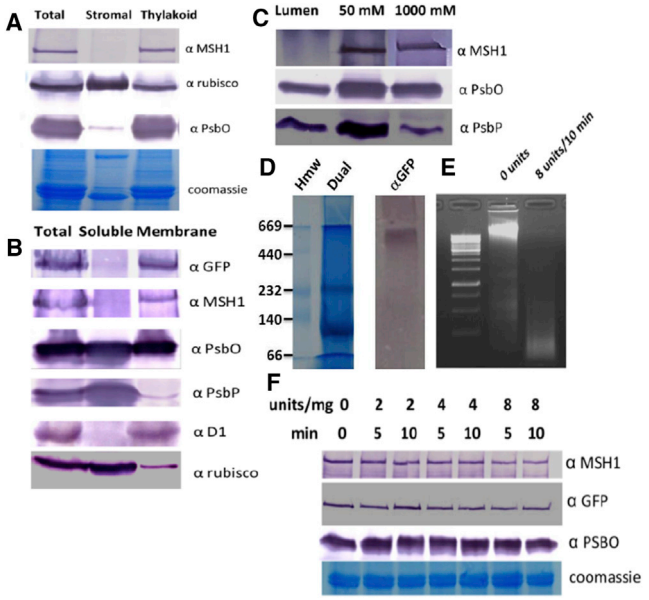

Figure 9. MSH1 Displays Evidence of Thylakoid Membrane Association.

(A) Test for MSH1 co-purification with the thylakoid membrane fraction in *Arabidopsis* plastid preparations, as shown by protein gel blot analysis.

(B and C) Tolerance of MSH1 membrane association to 0.1% Triton X-100 **(B)** and high-salt NaCl washes **(C)**.

(D) Non-denaturing polyacrylamide gel electrophoretic fractionation of thylakoid protein complexes and protein gel blot analysis with anti-GFP antibody reveals a high molecular weight complex between 440 and 669 kDa in size.

(E) MSH1 membrane association following nuclease digestion.

(F) DNA was precipitated from thylakoid membrane before (0 units) and after (8 units/10 min) nuclease treatment and fractionation in agarose gel. A representative Coomassie-stained gel in **(A)** and **(F)** is shown for loading control.

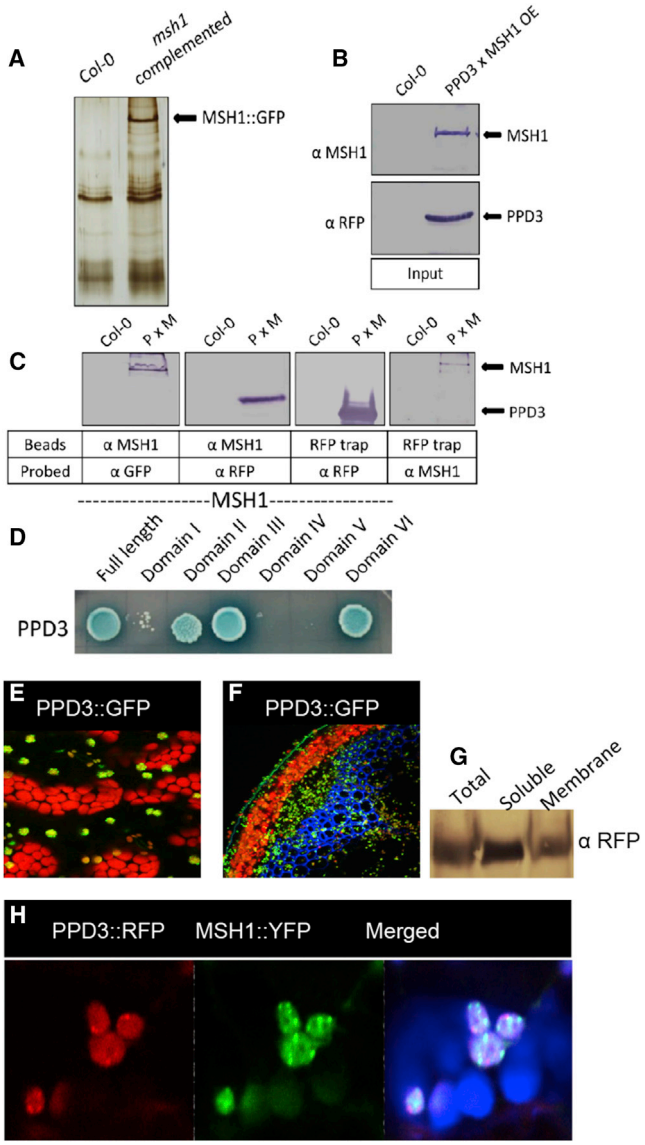

Figure 10. Physical Association of MSH1 with PPD3.

(A–C) Co-immunoprecipitation (coIP) from *Arabidopsis* stable transgenic lines expressing both MSH1::GFP and PPD3::RFP. Silver-stained gel showing a representative coIP precipitate **(A)**, input in sample **(B)**, and reciprocal coIP **(C)**.

(D) Yeast two-hybrid (one-on-one) assay showing PPD3-positive interaction with MSH1 at multiple domains within the MSH1 protein.

(E and F) Laser scanning confocal micrographs showing stable transgenic line expressing PPD3::GFP in epidermal (leaf lamina) **(E)** and stem vasculature (stem cross section) **(F)**. Xylem is imaged in blue.

(G) PPD3 in soluble and thylakoid membrane fractions, imaged by protein gel blot analysis with anti-RFP antibodies.

(H) Co-infiltration assay testing MSH1 and PPD3 co-localization on thylakoid membrane (diffuse signal). Note that punctate GFP (MSH1) signals are not co-aligned with PPD3 signal.

P × M represents PPD3 × MSH1 overexpression; MSH1::GFP = 150 kDa; PPD3::RFP = 52 kDa.

phenotypically normal *MSH1/msh1* heterozygote. In these experiments, crosses with the heterozygote as female, and either first- or second-generation *msh1/msh1* mutants as pollen donors, resulted in normal and enhanced-growth progeny. However, the reciprocal crosses, with the heterozygote as male, consistently resulted in a proportion (~10%–25%) of the progeny displaying a range of variegation, dwarfing, and delayed flowering similar to the *msh1* mutant (Figure 12). The frequency of *msh1*-like plants from crossing was far lower than would be expected by self-pollination of the *msh1* mutant. These results are consistent with our hypothesis that the *msh1* effect is an integrated organellar–epigenetic behavior.

The second experiment involved reciprocal crosses with an *msh1* mutant hemi-complemented with a mitochondrial-targeting form of *MSH1*. This line continues to express the *msh1* developmentally altered phenotype as a consequence of MSH1 depletion from the plastid (Supplemental Figure 12). The hemi-complemented line was crossed reciprocally to Col-0 wild-type, again showing a low and variable frequency of the *msh1* mutant phenotype when the hemi-complementation line was used as female, but no evidence of the mutant phenotype when used as pollen parent (Supplemental Figure 12B–12D). These data indicate that these reciprocal differences are the consequence of plastid influence.

DISCUSSION

The MSH1 effect, characterized by dramatic changes in development and stress response, as well as enhanced growth upon

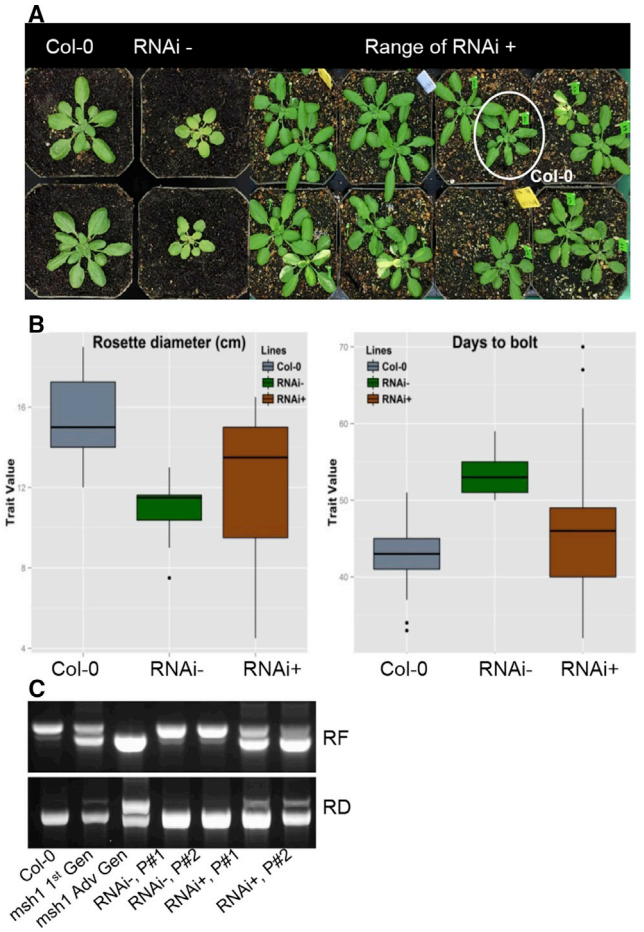

Figure 11. MSH1 RNAi Suppression Line Phenotype.
(A) Growth of RNAi− (without transgene) and RNAi+ (with transgene) compared with wild-type Col-0.
(B) Rosette diameter and days to bolt in RNAi− and RNAi+ lines compared with Col-0.
(C) Mitochondrial DNA recombination assay. Col-0 as a negative control; *msh1* first generation and *msh1* advanced generation as positive controls. P# denotes different plants.

crossing and grafting, is conserved among angiosperms (Xu et al., 2012; Santamaria et al., 2014; Virdi et al., 2015; Yang et al., 2015). The system serves as an excellent model for dissecting coordinate stress response networks within the plant. Gene expression changes in the *msh1* mutant integrate across a range of processes involving flowering time/vernalization, gibberellic acid catabolism, leaf morphology, maturity transition, cell cycle and growth rate, and abiotic stress responses (Shedge et al., 2010; Xu et al., 2011, 2012). Many of the processes perturbed in the *msh1* mutant are epigenetically modulated (reviewed by Bloomfield et al., 2014).

Results here, and from previous studies, suggest that the *msh1* reprogramming process is a plastid-driven phenomenon accompanied by mitochondrial genomic and epigenetic changes. The *msh1* phenotype integrates mitochondrial genome recombination which, at relatively low frequency, leads to altered leaf morphology and seed germination, heat tolerance, and male sterility (Sandhu et al., 2007), with plastid changes producing variegation, redox changes, variability in growth rate, and drought and light tolerance, together with epigenetic effects of uniform dwarfing, flowering delay, maturity delay, and a perennial growth behavior in short-day conditions.

Hemi-complementation and RNAi suppression studies show that these various phenotypes are a complex amalgamation resulting from depletion of a single multitargeting gene product. More importantly, the unusual range of *msh1* phenotypes, under conditions of chronic environmental stress, could represent a heritable adaptive response. While the relationship of organelle behavior with plant stress response is well documented, the integration of epigenetic effects with organellar perturbation is less so. Mammalian systems show interesting interplay of mitochondrial and nuclear epigenetic behavior (Figueroa et al., 2010; Castegna et al., 2015), but little if anything is known in plants of organellar triggers for non-stochastic epigenetic change.

The precise sub-compartmentation of MSH1 is elusive. Data are convincing for MSH1 as a nucleoid protein, and previous and present reports show MSH1 to influence both mitochondrial and plastid genome stability (Davila et al., 2011; Xu et al., 2011). We show that MSH1 function is affected by substitution of the signature phenylalanine (Phe-39) that characterizes the mismatch recognition motif of MutS homolog proteins (Malkov et al., 1997).

Protein–protein interaction data and physiological changes measured in the mutant argue for influence of MSH1 on redox regulation and stress response in the cell. Consistent with this interpretation, MSH1 associates with the plastid thylakoid membrane, and *MSH1* transcript levels are markedly reduced in plants under abiotic stress conditions (Shedge et al., 2010; Xu et al., 2011), a response that makes little sense when viewed in the context of organellar genome stability but is consistent with a role in environmental adaptation. Plastid nucleoid functions have been shown to be modulated by redox changes, leading to wider effects on gene expression (reviewed in Powikrowska et al., 2014). Consequently, we suggest that the *MSH1*-containing organelles behave as "sensory" plastids. Several studies have shown that vascular parenchyma and/or bundle-sheath plastids serve a signaling function to regulate mesophyll plastid behavior (Lundquist et al., 2014), consistent with our view that these unusual small plastids function as regulators.

Multifunctionality is relatively common in organellar proteins (Gancedo and Flores, 2008), particularly in nucleoid proteins (Kucej and Butow, 2007; Krupinska et al., 2013). One explanation for our observations is that MSH1 carries out two primary functions in the cell. In the meristem, MSH1 serves to suppress illegitimate recombination during prolific replication of organellar genomes. However, within epidermal and vascular parenchyma cells, MSH1 associates with the photosynthetic apparatus and/or plastoglobules on the photosynthetic membrane where *MSH1* disruption triggers heritable stress response in the plant.

The *MSH1* gene displays evidence of multifunctionalization during its evolution. The high degree of alignment of DNA binding and mismatch recognition motifs within domain I and the

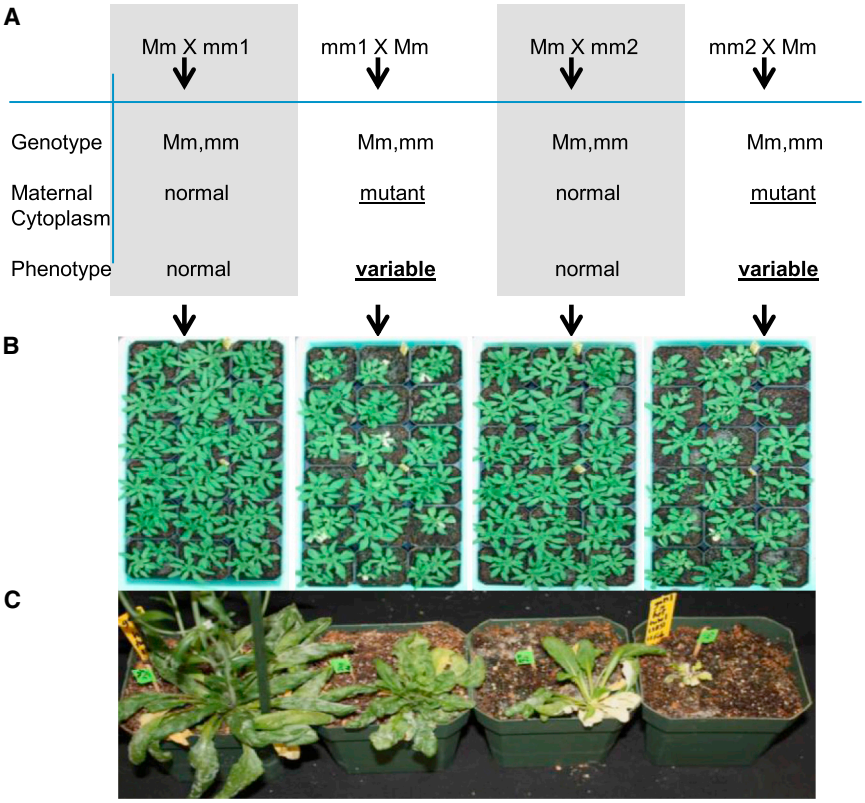

Figure 12. Maternal Inheritance of Phenotypic Range Determinants.

(A) Crossing scheme to determine contribution of genotype and cytoplasm to phenotype of progeny. *MSH1* heterozygous (Mm) TDNA lines were reciprocally crossed to homozygous first-generation (mm1) and second-generation (mm2) TDNA mutants.

(B) Photographs of segregating progeny, where progeny from heterozygous mothers appeared normal while progeny from mutant mothers displayed phenotypic variability regardless of progeny genotype.

(C) Like their homozygous mutant siblings, these heterozygous progeny from mm1 × Mm show variable size and flowering time.

ATPase of domain V suggest that MSH1 originated as a MutS homolog that, during its evolution, underwent fusion with a GIY-YIG class of homing endonuclease to enhance the protein's capacity for regulating recombination (Malik and Henikoff, 2000). MSH1 likely originated from the mitochondrion (Abdelnoor et al., 2006). Subsequent retargeting of the protein to the plastid may have facilitated acquisition of domains II, III, and IV, which encompass two hydrophobic intervals and potential sites of interaction with other thylakoid-localized proteins including PPD3. While PPD3 function has not been elucidated, it also appears to be associated with stress responses (Fey et al., 2005; Ifuku, 2014). Furthermore, ectopic expression of *MSH1* within mesophyll cells is not tolerated, further underlining the specialized properties of the protein.

Physiological changes in *msh1* are characteristic of altered redox state and plastoglobule response (Zbierzak et al., 2009; Piller et al., 2014). Measurable enhancement of these effects within the stem tissues, where *MSH1* expression is more concentrated, is consistent with localization to sensory plastids. The vascular tissue association of MSH1 may also account for the graft transmissibility of effects arising from its depletion (Virdi et al., 2015). The plastoglobule, where much of the *msh1*-associated physiological response occurs, is a suborganellar compartment that participates in stress signaling and senescence (Kessler and Vidi, 2007; Singh and McNellis, 2011; Besagni and Kessler, 2013). Our working model involves marked changes within the plastoglobule during *MSH1* depletion that trigger the signal for nuclear epigenetic response. Recently, plastidial redox signals were shown to participate in epigenetic control (Dietzel et al., 2015) and in generating mobile signals in vasculature (Petrillo et al., 2014).

Assuming an association exists between the redox changes described in this study and nuclear epigenetic response, we are interested to learn whether similar epigenetic responses arise with the low-frequency mitochondrial perturbations that condition wrinkled and curly leaf phenotypes. The unusual mitochondrial variants produce similar redox-modulating behaviors, and appear to condition enhanced-growth phenotypes through crossing. Although the *msh1* cellular behavior collectively resembles a plant undergoing senescence (Besagni and Kessler, 2013), the *msh1* mutant is green and completes successful flowering and formation of viable seed. It is, perhaps, this mistimed condition of senescence-like physiological behavior under conditions of continued plant growth that leads to programmed epigenetic changes.

Evidence of heritable, non-genetic changes in the plant (Santamaria et al., 2014; Virdi et al., 2015; Yang et al., 2015), following *MSH1* depletion, reflects either direct or indirect influence of the protein on nuclear genome behavior. We have no evidence for direct interaction of MSH1 in the nuclear genome, but we have not formally eliminated the possibility of plastid–nuclear interaction. Unusual intracellular plastid–nuclear behavior has been suggested to occur for WHIRLY1 protein (Grabowski et al., 2008), also a nucleoid, multitargeting, and multifunctional organellar protein, and plastid stromules have been demonstrated to participate in cellular plant stress behavior, perhaps constituting a direct conduit of plastid–nuclear communication (Caplan et al., 2015).

We previously showed in several plant species that *MSH1* depletion produces a complex and programmed alteration in plant phenotype. The present study dissects this developmental reprogramming phenotype into its mitochondrial, plastidial, and epigenetic components, and links the effects to a specialized spatial pattern and plastid type. It is unclear how initial cellular perturbations arising with MSH1 depletion are transformed into heritable epigenetic changes, although we show that these processes are largely directed via the plastid and, remarkably, that the epigenetic component of the reprogramming process is

subsequently separable from the organellar one. This advancement should now allow us to test for a small RNA component sufficient to condition these dissected epigenetic changes, and to begin to understand how organellar and epigenetic behaviors integrate to affect growth.

METHODS

Plant Materials

Arabidopsis thaliana Col-0 was obtained from Lehle Seed Company. Heterozygous plants for complementation experiments were generated by conventional crossing using Col-0 as a female (Col-0 × chm1-1). MSH1 fully and hemi-complemented *Arabidopsis* transgenic lines were advanced from the Xu et al. (2011) study. The TDNA mutants were obtained from TAIR (http://www.arabidopsis.org/): *msh1* (SAIL-877-F01), *ppd3*-sail (SAIL-641-C02), and *ppd3*-gabi (GK-121C07). Genotyping primers are listed in Supplemental Table 6. Plants were grown in standard growth conditions at 22°C under long-day (16 h light/8 h dark) or short-day (12 h light/12 h dark) photoperiods in a walk-in chamber. MSH1 RNAi materials were developed as described by Virdi et al. (2015).

Plasmid Construction for *Arabidopsis* Transgenic Plants and Tobacco Infiltration Experiments

For GUS (β-glucuronidase) fusion expression constructs, MSH1 full-length genomic DNA (gDNA) with its native promoter was ligated to pBI101 promoter-less binary vector. MSH1 DNA binding mutant constructs were created by serial cloning. Full-length MSH1 gDNA with native promoter was ligated to intermediate vector pBlueScript (KS+). Site-directed mutagenesis was carried out with primers specific for FYE/LYE, FYE/FCA, FYE/FYA, and triple mutation FYE/LCA with the QuikChange Site-Directed Mutagenesis Kit (Stratagene) according to the manufacturer's instructions. Mutated fragments from the intermediate vector were transferred to plant binary vector pCambia1302C lacking 35S promoter. For reporter clones, the first 88 amino acids of PEND and full-length gDNA of pTAC2, MFP1, PPD3, PSBO1, PSBO2, PetC, and Tic55 were ligated to mGFP and mRFP versions of pCambia1302C. Full-length gDNA MSH1 was also ligated to the pFAST::eYFP vector for some of the co-localization experiments. Truncated versions of MSH1 were ligated to the mGFP version of pCambia1302C. For the construction of the nuclear targeted MSH1 clone, NLS sequence was derived from the class 5 plant-specific NLS sequence (b54) (Kosugi et al., 2009) and cloned into an intermediate vector pBluescript (SK+) carrying MSH1 native promoter and the full-length gene without the organelle targeting presequence (ATG −77aa). NLS sequence was inserted between the promoter and the gene in-frame. This was then moved into the binary vector pCAMBIA1302C::GFP for plant experiments.

All PCR amplifications were carried out with Phusion High-Fidelity DNA polymerase according to the manufacturer's instructions (Thermo Scientific, catalog #F-530L). Restriction enzymes were purchased from New England Biolabs. Gel extractions and plasmid preparations were done with Qiagen kits. *Arabidopsis* transgenic stable lines were generated by the floral-dip method (Clough and Bent, 1998).

The tobacco transient infiltration assay was carried out as described by Van den Ackerveken et al. (1996). In brief, a 5-ml culture of agrobacteria with antibiotic was grown overnight, centrifuged, and resuspended in 6 ml of induction media with antibiotic and 50 μm of acetosyringone, and grown for another 6–8 h. Bacteria were centrifuged and resuspended in infiltration media to 0.8 OD and 150 μm acetosyringone. Bacterial culture was then infiltrated with a needle-less syringe on the abaxial side of tobacco (*Nicotiana benthamiana*) leaves. For co-infiltration assay, each construct was grown and kept separate until resuspension in infiltration media. Two cultures were mixed 1:1 before infiltrating tobacco leaves. Leaves were visualized by laser scanning confocal microscopy 36 h after infiltration. All primers for cloning are listed in Supplemental Table 5.

Genetic Complementation Experiments

Genetic complementation was conducted as described by Xu et al. (2011). In brief, *MSH1/msh1* plants derived from Col-0 × *chm1-1* were floral dipped, and T1 seeds were selected on hygromycin selection plates (30 μg/ml) and genotyped for *msh1/msh1*, transgene-positive segregants. Complementation was assayed by variegation, delayed flowering, and mitochondrial DNA recombination phenotypes in T1 and T2 plants under short-day photoperiod growth conditions.

GUS Expression and Staining

GUS staining was done as described by Jefferson (1987), and destaining was done as described by Stangeland and Salehian (2002) with some modifications. In brief, after GUS staining the samples were destained for 1 h in ethanol/acetic acid (1:1) and then further destained in 70% ethanol with several changes for 12 h. Samples were examined with an Olympus AX70 microscope and photographs were taken with an Olympus DP25 camera.

Laser Scanning Confocal Microcopy

For *Arabidopsis* stable transformed plants, leaf lamina and vein areas were visualized for epidermal, mesophyll, and vascular parenchyma cells. For the tobacco transient assay, infiltrated leaves were incubated for 36 h before imaging. All imaging for GFP, RFP, and yellow fluorescent protein (YFP) were performed on the Nikon A1 confocal laser scanning microscope mounted on the Nikon Eclipse 90 upright compound microscope. Image acquisition used Nikon NIS Elements version 4.20. GFP (excitation: 488 nm; emission: 500–550 nm), RFP (excitation: 561.4 nm; emission: 570–620 nm), YFP (excitation: 514.5 nm; emission: 525–555 nm), and chlorophyll autofluorescence (excitation: 640.6 nm; emission: 663–738 nm) images were acquired sequentially or simultaneously where appropriate.

Transmission Microscopy

Leaf samples for transmission electron microscopy were prepared as follows. Leaf samples from green lamina and midrib of 3-week-old *chm1-1* mutant and wild-type plants were dissected and fixed in 2.5% glutaraldehyde in 0.05 M sodium cacodylate (pH 7.4) and postfixed in 1% osmium tetroxide in 0.05 M sodium cacodylate (pH 7.4) for 2 h. Samples were dehydrated in a graduated ethanol series and embedded in Epon 812 (Electron Microscopic Sciences). Thin sections (80 nm) were stained by uranyl acetate and lead citrate, and observed under a transmission electron microscope (Hitachi H7500-I) at the University of Nebraska Center for Biotechnology Microscopy Facility.

Yeast Two-Hybrid Experiments

MSH1 full-length gene from cDNA was cloned in the pGBKT7 two-hybrid DNA BD vector. For the library, total RNA was isolated from floral tissues of *Arabidopsis* Col-0, and purified mRNA was obtained using the Nucleotrap mRNA kit from Clontech. The yeast two-hybrid library was made in pGADT7 AD vector using the Matchmaker library construction and screening kit according to protocols provided by the manufacturer (Clontech). Positive interaction partners were isolated and identified by sequencing. Further testing of interaction was done by one-to-one mating with *MSH1* on rich media and transferred to synthetic dropout plates, first plated on SD-Leu-Trp to confirm the presence of both bait and fish and then on SD-Leu-Trp-His-Ade X-alpha-gal plates for blue color development for positive interactions. The second more stringent screen was done by developing a yeast two-hybrid library from *A. thaliana* ecotype Col-0 stem tissue using the Make Your Own "Mate & Plate" Library System (Clontech cat. #630490). This library was screened with MSH1 as bait using the more stringent yeast two-hybrid screen Matchmaker Gold Yeast Two-Hybrid System (Clontech cat. #630489).

Mass Spectrometry

Tandem mass spectrometry was performed at the University of Nebraska Mass Spectrometry Core Facility using a Waters Q-TOF Ultima mass

spectrometer (Waters; formally Micromass). Results were analyzed using the Mascot software package (Matrix Science).

Plastid and Thylakoid Preparation, and Nuclease Treatment for MSH1 Topology Experiments

Crude plastids were prepared as described by Hall et al. (2011). In brief, 4-week-old plants were ground in chloroplast extraction buffer (20 mM Tricine–NaOH [pH 8.0], 300 mM sorbitol, 10 mM KCl, 10 mM EDTA, 0.25% BSA, 4.5 mM sodium ascorbate, 5 mM L-cysteine) centrifuged at 3000 *g* for 10 min at 4°C. Pellet was washed twice with wash buffer (20 mM HEPES–NaOH [pH 7.8], 300 mM sorbitol, 10 mM KCl, 2.5 mM EDTA, and 5 mM $MgCl_2$), resuspended in the same buffer at 1 mg/ml chlorophyll concentration, and stored at −80°C. For thylakoid preparation, fresh resuspended plastids were lysed osmotically with osmotic shock buffer (10 mM sodium pyrophosphate–NaOH [pH 7.8], 1× Sigma protease inhibitor cocktail) and kept for 30 min at 4°C. Stromal proteins were separated at 100 000 *g* for 1 h, and the thylakoid pellet was washed with thylakoid wash buffer 1 (2 mM Tricine–HCl [pH 7.8], 300 mM sucrose) and buffer II (2 mM Tricine–HCl [pH 7.8], 100 mM sucrose, 50 mM NaCl, 5 mM $MagCl_2$, 1 mM EDTA), resuspended in wash buffer II, and aliquoted at 1 mg/ml chlorophyll concentration. Isolated thylakoids were treated with micrococcal nuclease (Sigma) in digestion buffer (25 mM HEPES [pH 8.0], 5 mM $MgCl_2$, 20 mM NaCl, 1× Sigma protease inhibitor cocktail without EDTA) at specified time and concentrations, and washed with thylakoid wash buffer II. Nucleoids were precipitated from nuclease-treated and -untreated thylakoids using the chloroform/phenol DNA extraction method. For SDS–PAGE, crude plastids or thylakoids were lysed with resuspension buffer containing 1% Triton for 1 h and centrifuged at 20 000 *g* for 1 h at 4°C. Cleared lysate was used for further analysis.

Chloroplast Chromatin Immunoprecipitation Assay

Chloroplast ChIP assay was performed as described by Yagi et al. (2012). In brief, crude plastids were cross-linked with formaldehyde 1% (v/v) in chloroplast isolation buffer and incubated at 25°C for 10 min. Cross-linking reaction was stopped with 150 μl of 1 M glycine for 25°C for 5 min and washed with chloroplast isolation buffer. Cross-linked plastids were lysed and incubated with GFP-Trap beads, and DNA–protein complex was eluted, reverse cross-linked with 8 μl of 5 M NaCl and 2 μl of 10 mg/ml Proteinase K in elution fraction, and incubated at 65°C overnight. Immunoprecipitated DNA was purified with a PCR purification kit according to the manufacturer's instructions. Detailed protocol and buffers are as described by Yagi et al. (2012). PCR was performed with 1 μl of DNA and run in 1% agarose gel.

Protein Preparation, Co-immunoprecipitation, and Immunoblots

Leaves were ground in liquid nitrogen and total proteins were extracted with lysis buffer (50 mM sodium phosphate buffer [pH 7.0], 10 mM EDTA, 1% Triton, 0.1% sodium lauryl sarcosine, 1× protease inhibitor, and freshly added 7 μl of β-mercaptoethanol/10 ml) for 1 h at 4°C and centrifuged at 20 000 *g* for 1 h. Cleared supernatant was used for immunoblot assay. Plastid proteins were prepared as described above. For coIP, anti-MSH1 beads were prepared with Pierce NHS activated agarose and GlycoLink purified MSH1 antibody. Anti-GFP (ab69314) agarose beads was purchased from Abcam, while GFP-Trap A (gta-10) and RFP-Trap A (rta-10) beads were purchased from ChromoTek. Total protein was extracted with buffer (100 mM Tris–HCl [pH 7.8], 100 mM NaCl, 0.1% NP40, 1 mM $MgCl_2$, 1 mM $CaCl_2$, and 1× protease inhibitor cocktail without EDTA). Antibody beads were incubated with protein lysate overnight, washed three times with wash buffer (100 mM Tris–HCl [pH 7.8], 50 mM NaCl, 0.05% NP40, 1 mM $MgCl_2$, 1 mM $CaCl_2$, and 1× protease inhibitor cocktail without EDTA), and proteins were eluted with 2× SDS loading buffer.

Fluorescence-Activated Cell Sorting Analysis

Crude plastids from leaves and inflorescence stems were prepared as described above. Resuspended plastids were cleared through 5-ml polystyrene round-bottomed tubes with cell strainer caps. Plastid suspensions were analyzed by flow cytometry using a FACS Aria II SORP (BD Biosciences) with PBS as a sheath fluid. A 488-nm laser was used for excitation, and emission was measured at 530/30 nm for GFP and 685/35 nm for chlorophyll. Data were collected using FACSDiva 6.1.3 software (BD Biosciences), and analyzed using FlowJo version 7.6.3 (TreeStar). Protoplasts were defined by positive signal in the 685/35 detector versus FSC-A, then analyzed for GFP expression in the plot of 530/30 versus 685/35.

Quantification of Plastoquinone-9, Plastochromanol-8, and α-Tocopherol

Arabidopsis leaves and inflorescence stems (10–30 mg of fresh weight) were homogenized in 1 ml of 100% methanol using a 5-ml Pyrex tissue grinder. Extracts were cleared by centrifugation (18 000 *g* for 5 min) and analyzed by high-performance liquid chromatography with diode array (plastoquinone-9) or fluorescence detection (plastoquinol-9, α-tocopherol, plastochromanol-8) as previously described (Block et al., 2013). Retention times were 6.6 min (α-tocopherol), 14.3 min (plastoquinol-9), 28.4 min (plastochromanol-8), and 40.7 min (plastoquinone-9). Metabolites were quantified according to their corresponding external calibration standards as previously described (Block et al., 2013).

Quantification of Non-photochemical Quenching Rates

Non-photochemical quenching rates were measured as previously described (Roose et al., 2011, 2014; Bricker et al., 2014).

SUPPLEMENTAL INFORMATION

Supplemental Information is available at *Molecular Plant Online*.

FUNDING

We gratefully acknowledge support from the Division of Chemical Sciences, Geosciences, and Biosciences, Office of Basic Energy Sciences of DOE (DE-FG02-10ER16189 and DE-FG02-98ER20310 [for the photosynthetic measurements]) for this research, with support from the Bill and Melinda Gates Foundation (OPP1088661) for the genetic analyses.

AUTHOR CONTRIBUTIONS

K.S.V., S.L., T.E., and P.M.D. were responsible for genetic and biochemical assays, Y.W., K.S.V., and C.E. carried out protein interaction and confocal studies. K.S.V. performed coIP and chloroplast ChIP assay. J.D.L. and K.S.V. participated in reciprocal crossing studies. Y.W., K.S.V., and H.K. carried out genetic and mutation studies. H.K. carried out MSH1 RNAi evaluation. S.K. and K.S.V. participated in nested deletion targeting. K.S.V., A.B., G.B., T.B., and J.L.R. participated in redox and photosynthesis analyses. K.S.V. and I.K. participated in flow cytometry and sensory plastid analysis. S.M. planned the research, participated in experimental design and drafted the manuscript.

ACKNOWLEDGMENTS

We thank Dr. Han Chen and the Center for Biotechnology Microscopy Facility for assistance with electron and confocal microscopy, Omar Lozano for technical assistance, Eric and Scott Latimer for assisting quantification of stem metabolites with high-performance liquid chromatography, Vikas Shedge for guiding the heat treatment experiment, and Danielle Shea for technical assistance with FACS analysis. S. Mackenzie serves as a scientific consultant to EpiCrop Technologies, an epigenetic breeding company.

Received: August 23, 2015
Revised: October 20, 2015
Accepted: October 29, 2015
Published: November 14, 2015

REFERENCES

Abdelnoor, R.V., Yule, R., Elo, A., Christensen, A.C., Meyer-Gauen, G., and Mackenzie, S.A. (2003). Substoichiometric shifting in the plant mitochondrial genome is influenced by a gene homologous to MutS. Proc. Natl. Acad. Sci. USA **100**:5968–5973.

Abdelnoor, R.V., Christensen, A.C., Mohammed, S., Munoz-Castillo, B., Moriyama, H., and Mackenzie, S.A. (2006). Mitochondrial genome dynamics in plants and animals: convergent gene fusions of a MutS homologue. J. Mol. Evol. **63**:165–173.

Arrieta-Montiel, M.P., Shedge, V., Davila, J., Christensen, A.C., and Mackenzie, S.A. (2009). Diversity of the Arabidopsis mitochondrial genome occurs via nuclear-controlled recombination activity. Genetics **183**:1261–1268.

Besagni, C., and Kessler, F. (2013). A mechanism implicating plastoglobules in thylakoid disassembly during senescence and nitrogen starvation. Planta **237**:463–470.

Bilichak, A., Ilnystkyy, Y., Hollunder, J., and Kovalchuk, I. (2012). The progeny of *Arabidopsis thaliana* plants exposed to salt exhibit changes in DNA methylation, histone modifications and gene expression. PLoS One **7**:e30515.

Block, A., Fristedt, R., Rogers, S., Kumar, J., Barnes, B., Barnes, J., Elowsky, C.G., Wamboldt, Y., Mackenzie, S.A., Redding, K., et al. (2013). Functional modeling identifies paralogous solanesyl-diphosphate synthases that assemble the side chain of plastoquinone-9 in plastids. J. Biol. Chem. **288**:27594–27606.

Bloomfield, J.A., Rose, T.J., and King, G.J. (2014). Sustainable harvest: managing plasticity for resilient crops. Plant Biotechnol. J. **12**:517–533.

Bricker, T.M., Roose, J.L., Zhang, P., and Frankel, L.K. (2013). The PsbP family of proteins. Photosynth. Res. **116**:235–250.

Bricker, T.M., Bell, A.J., Tran, L., Frankel, L.K., and Theg, S.M. (2014). Photoheterotrophic growth of *Physcomitrella patens*. Planta **239**:605–613.

Bond, D.M., and Baulcombe, D.C. (2014). Small RNAs and heritable epigenetic variation in plants. Trends Cell Biol. **24**:100–107.

Boyko, A., Blevins, T., Yao, Y., Golubov, A., Bilichak, A., Ilnytskyy, Y., Hollunder, J., Meins, F., Jr., and Kovalchuk, I. (2010). Transgenerational adaptation of *Arabidopsis* to stress requires DNA methylation and the function of dicer-like proteins. PLoS One **5**:e9514.

Caplan, J.L., Kumar, A.S., Park, E., Padmanabhan, M.S., Hoban, K., Modia, S., Czymmek, K., and Dinesh-Kumar, S.P. (2015). Chloroplast stromules function during innate immunity. Dev. Cell **34**:1–15.

Castegna, A., Iacobazzi, V., and Infantino, V. (2015). The mitochondrial side of epigenetics. Physiol. Genomics **47**:299–307.

Clough, S.J., and Bent, A.F. (1998). Floral dip: a simplified method for *Agrobacterium*-mediated transformation of *Arabidopsis thaliana*. Plant J. **16**:735–743.

Davila, J.I., Arrieta-Montiel, M.P., Wamboldt, Y., Cao, J., Hagmann, J., Shedge, V., Xu, Y.Z., Weigel, D., and Mackenzie, S.A. (2011). Double-strand break repair processes drive evolution of the mitochondrial genome in *Arabidopsis*. BMC Biol. **9**:64.

Dietzel, L., Gläßer, C., Liebers, M., Hiekel, S., Courtois, F., Czarnecki, O., Schlicke, H., Zubo, Y., Börner, T., Mayer, K., et al. (2015). Identification of early nuclear target genes of plastidial redox signals that trigger the long-term response of *Arabidopsis* to light quality shifts. Mol. Plant **8**:1237–1252.

Eichten, S.R., Schmitz, R.J., and Springer, N.M. (2014). Epigenetics: beyond chromatin modifications and complex genetic regulation. Plant Physiol. **165**:933–947.

Fey, V., Wagner, R., Brauetigam, K., Wirtz, M., Hell, R., Dietzmann, A., Leister, D., Oelmueller, R., and Pfannschmidt, T. (2005). Retrograde plastid redox signals in the expression of nuclear genes for chloroplast proteins of *Arabidopsis thaliana*. J. Biol. Chem. **280**:5318–5328.

Figueroa, M.E., Abdel-Wahab, O., Lu, C., Ward, P.S., Patel, J., Shih, A., Li, Y., Bhagwat, N., Vasanthakumar, A., Fernandez, H.F., et al. (2010). Leukemic IDH1 and IDH2 mutations result in a hypermethylation phenotype, disrupt TET2 function, and impair hematopoietic differentiation. Cancer Cell **18**:553–567.

Friso, G., Giacomelli, L., Ytterberg, A.J., Peltier, J.B., Rudella, A., Sun, Q., and Van Wijk, K.J. (2004). In-depth analysis of the thylakoid membrane proteome of *Arabidopsis thaliana* chloroplasts: new proteins, new functions, and a plastid proteome database. Plant Cell **16**:478–499.

Fristedt, R., Herdean, A., Blaby-Haas, D.E., Mamedov, F., Merchant, S.S., Last, R.L., and Lundin, B. (2015). PHOTOSYSTEM II PRROTEIN33, a protein conserved in the plastid lineage, is associated with the thylakoid membrane and provides stability to photosystem II supercomplexes in *Arabidopsis*. Plant Physiol. **167**:481–492.

Gancedo, C., and Flores, C.L. (2008). Moonlighting proteins in yeasts. Microbiol. Mol. Biol. Rev. **72**:197–210.

Grabowski, E., Miao, Y., Mulisch, M., and Krupinska, K. (2008). Single-stranded DNA-binding protein in barley leaves is located in plastids and the nucleus of the same cell. Plant Physiol. **147**:1800–1804.

Hall, M., Mishra, Y., and Schröder, W.P. (2011). Preparation of stroma, thylakoid membrane, and lumen fractions from *Arabidopsis thaliana* chloroplasts for proteomic analysis. Methods Mol. Biol. **775**:207–222.

Hu, J., Huang, W., Huang, Q., Qin, X., Yu, C., Wang, L., Li, S., Zhu, R., and Zhu, Y. (2014). Mitochondria and cytoplasmic male sterility in plants. Mitochondrion **19 Pt B**:282–288.

Ifuku, K. (2014). The PsbP and PsbQ family proteins in the photosynthetic machinery of chloroplasts. Plant Physiol. Biochem. **81**:108–114.

Jacoby, R.P., Li, L., Huang, S., Pong Lee, C., Millar, A.H., and Taylor, N.L. (2012). Mitochondrial composition, function and stress response in plants. J. Integr. Plant Biol. **54**:887–906.

Jefferson, R.A. (1987). Assaying chimeric genes in plants: the GUS gene fusion system. Plant Mol. Biol. Rep. **5**:387.

Kessler, F., and Vidi, P.A. (2007). Plastoglobule lipid bodies: their functions in chloroplasts and their potential for applications. Adv. Biochem. Eng. Biotechnol. **107**:153–172.

Kim, M., Lee, U., Small, I., des Francs-Small, C.C., and Vierling, E. (2012). Mutations in an *Arabidopsis* mitochondrial transcription termination factor-related protein enhance thermotolerance in the absence of the major molecular chaperone HSP101. Plant Cell **24**:3349–3365.

Krupinska, K., Melonek, J., and Krause, K. (2013). New insights into plastid nucleoid structure and functionality. Planta **237**:653–664.

Kucej, M., and Butow, R.A. (2007). Evolutionary tinkering with mitochondrial nucleoids. Trends Cell Biol. **17**:586–592.

Lundquist, P.K., Rosar, C., Brautigam, A., and Weber, A.P. (2014). Plastid signals and the bundle sheath: mesophyll development in reticulate mutants. Mol. Plant **7**:14–29.

Malik, H.S., and Henikoff, S. (2000). Dual recognition-incision enzymes might be involved in mismatch repair and meiosis. Trends Biochem. Sci. **25**:414–418.

Malkov, V.A., Biswas, I., Camerini-Otero, R.D., and Hsieh, P. (1997). Photocross-linking of the NH2-terminal region of Taq MutS protein to the major groove of a heteroduplex DNA. J. Biol. Chem. **272**:23811–23817.

Kosugi, S., Hasebe, M., Matsumura, N., Takashima, H., Miyamoto-Sato, E., Tomita, M., and Yanagawa, H. (2009). Six classes of

nuclear localization signals specific to different binding grooves of importin alpha. J. Biol. Chem. **284**:478–485.

Melnyk, C.W., Molnar, A., Bassett, A., and Baulcombe, D.C. (2011). Mobile 24 nt small RNAs direct transcriptional gene silencing in the root meristems of *Arabidopsis thaliana*. Curr. Biol. **21**:1678–1683.

Pecinka, A., Dinh, H.Q., Baubec, T., Rosa, M., Lettner, N., and Mittelsten Scheid, O. (2010). Epigenetic regulation of repetitive elements is attenuated by prolonged heat stress in *Arabidopsis*. Plant Cell **22**:3118–3129.

Petrillo, E., Godoy Herz, M.A., Fuchs, A., Reifer, D., Fuller, J., Yanovsky, M.J., Simpson, C., Brown, J.W.S., Barta, A., Kalyna, M., et al. (2014). A chloroplast retrograde signal regulates nuclear alternative splicing. Science **344**:427–430.

Pfalz, J., Liebers, M., Hirth, M., Grübler, B., Holtzegel, U., Schröter, Y., Dietzel, L., and Pfannschmidt, T. (2012). Environmental control of plant nuclear gene expression by chloroplast redox signals. Front Plant Sci. **3**:257.

Piller, E.L., Glauser, G., Kessler, F., and Besagni, C. (2014). Role of plastoglobules in metabolite repair in the tocopherol redox cycle. Front. Plant Sci. **5**:298.

Powikrowska, M., Oetke, S., Jensen, P.E., and Krupinska, K. (2014). Dynamic composition, shaping and organization of plastid nucleoids. Front Plant Sci. **5**:424.

Rolland, N., Curien, G., Finazzi, G., Kuntz, M., Maréchal, E., Matringe, M., Ravanel, S., and Seigneurin-Berny, D. (2012). The biosynthetic capacities of the plastids and integration between cytoplasmic and chloroplast processes. Annu. Rev. Genet. **46**:233–264.

Roose, J.L., Frankel, L.K., and Bricker, T.M. (2011). Developmental defects in mutants of the PsbP domain protein 5 in *Arabidopsis thaliana*. PLoS One **6**:e28624.

Roose, J.L., Frankel, L.K., and Bricker, T.M. (2014). The PsbP domain protein 1 functions in the assembly of lumenal domains in photosystem I. J. Biol. Chem. **289**:23776–23785.

Sandhu, A.P., Abdelnoor, R.V., and Mackenzie, S.A. (2007). Transgenic induction of mitochondrial rearrangements for cytoplasmic male sterility in crop plants. Proc. Natl. Acad. Sci. USA **104**:1766–1770.

Santamaria, R., Shao, M.-R., Wang, G., Nino-Liu, D.O., Kundariya, H., Wamboldt, Y., Dweikat, I., and Mackenzie, S. (2014). Implementing selection of MSH1-induced non-genetic variation in *Sorghum bicolor* as a model for epigenetic breeding in crops. PLoS One **9**:e108407.

Schwarzländer, M., and Finkemeier, I. (2013). Mitochondrial energy and redox signaling in plants. Antioxid. Redox Signal. **18**:2122–2144.

Shedge, V., Davila, J., Arrieta-Montiel, M.P., Mohammed, S., and Mackenzie, S.A. (2010). Extensive rearrangement of the *Arabidopsis* mitochondrial genome elicits cellular conditions for thermotolerance. Plant Physiol. **152**:1960–1970.

Shivaprasad, P.V., Dunn, R.M., Santos, B.A., Bassett, A., and Baulcombe, D.C. (2012). Extraordinary transgressive phenotypes of hybrid tomato are influenced by epigenetics and small silencing RNAs. EMBO J. **31**:257–266.

Singh, D.K., and McNellis, T.W. (2011). Fibrillin protein function: the tip of the iceberg? Trends Plant Sci. **16**:432–441.

Stangeland, B., and Salehian, Z. (2002). An improved clearing method for GUS assay in *Arabidopsis* endosperm and seeds. Plant Mol. Biol. Rep. **20**:107–114.

Terasawa, K., and Sato, N. (2005). Visualization of plastid nucleoids in situ using the PEND-GFP fusion protein. Plant Cell Physiol. **46**:649–660.

Tsai, H.-L., Lue, W.-L., Lu, K.-J., Hsieh, M.-H., Wang, S.-M., and Chen, J. (2009). Starch synthesis in *Arabidopsis* is achieved by spatial cotranscription of core starch metabolism genes. Plant Physiol. **151**:1585–1595.

Van den Ackerveken, G., Marois, E., and Bonas, U. (1996). Recognition of the bacterial avirulence protein AvrBs3 occurs inside the host plant cell. Cell **87**:1307–1316.

Vidi, P.-A., Kanwischer, M., Baginsky, S., Austin, J.R., Csucs, G., Dörmann, P., Kessler, F., and Bréhélin, C. (2006). Tocopherol cyclase (VTE1) localization and vitamin E accumulation in chloroplast plastoglobule lipoprotein particles. J. Biol. Chem. **281**:11225–11234.

Virdi, K.S., Laurie, J.D., Xu, Y.-Z., Yu, J., Shao, M.-R., Sanchez, R., Kundariya, H., Wamboldt, Y., Wang, D., Riethoven, J.-J., et al. (2015). *Arabidopsis* MSH1 mutation alters the epigenome to produce heritable changes in plant growth. Nat. Comm. **6**:6386.

Xu, Y.Z., Arrieta-Montiel, M.P., Virdi, K.S., de Paula, W.B., Widhalm, J.R., Basset, G.J., Davila, J.I., Elthon, T.E., Elowsky, C.G., Sato, S.J., et al. (2011). MUTS HOMOLOG1 is a nucleoid protein that alters mitochondrial and plastid properties and plant response to high light. Plant Cell **23**:3428–3441.

Xu, Y.Z., Santamaria Rde, L., Virdi, K.S., Arrieta-Montiel, M.P., Razvi, F., Li, S., Ren, G., Yu, B., Alexander, D., Guo, L., et al. (2012). The chloroplast triggers developmental reprogramming when MUTS HOMOLOG1 is suppressed in plants. Plant Physiol. **159**:710–720.

Yagi, Y., Ishizaki, Y., Nakahira, Y., Tozawa, Y., and Shiina, T. (2012). Eukaryotic-type plastid nucleoid protein pTAC3 is essential for transcription by the bacterial-type plastid RNA polymerase. Proc. Natl. Acad. Sci. USA **109**:7541–7546.

Yang, X., Kundariya, H., Xu, Y.Z., Sandhu, A., Yu, J., Hutton, S.F., Zhang, M., and Mackenzie, S.A. (2015). MSH1-Derived epigenetic breeding potential in tomato. Plant Physiol. **168**:222–232.

Ytterberg, A.J., Peltier, J.B., and van Wijk, K.J. (2006). Protein profiling of plastoglobules in chloroplasts and chromoplasts. A surprising site for differential accumulation of metabolic enzymes. Plant Physiol. **140**:984–997.

Zbierzak, A.M., Kanwischer, M., Wille, C., Vidi, P.A., Giavalisco, P., Lohmann, A., Briesen, I., Porfirova, S., Bréhélin, C., Kessler, F., et al. (2009). Intersection of the tocopherol and plastoquinol metabolic pathways at the plastoglobule. Biochem. J. **425**:389–399.